Investigation on long-term progressive deformation of engineering slope based on comprehensive monitoring

Shi-shu ZHANG, Song-feng GUO, Sheng-wen QI, Feng-jiao TANG, Jin-shan HU, Xiao-ping ZHAO, Cong-yan RAN, Xin WANG, Yu ZOU, Xiao-lin HUANG, Bo-wen ZHENG, Ning LIANG

Articles you may be interested in

Deformation and failure mechanism of Yanjiao rock slope influenced by rainfall and water level fluctuation of the Xiluodu hydropower station reservoir

Journal of Mountain Science. 2023, 20(1): 1   https://doi.org/10.1007/s11629−022−7755−0

Failure mechanism of a large−scale composite deposits caused by the water level increases

Journal of Mountain Science. 2023, 20(5): 1369   https://doi.org/10.1007/s11629−022−7690−1

Deformation of the Zhangjiazhuang high−speed railway tunnel: an analysis of causal mechanisms using geomorphological surveys and D−InSAR monitoring

Journal of Mountain Science. 2021, 18(7): 1920   https://doi.org/10.1007/s11629−020−6493−5

Slope stability evaluation and monitoring of a landslide: a case study from NE Turkey

Journal of Mountain Science. 2020, 17(11): 2624   https://doi.org/10.1007/s11629−020−6306−x

Influence of excavation schemes on slope stability: A DEM study

Journal of Mountain Science. 2020, 17(6): 1509   https://doi.org/10.1007/s11629−019−5605−6

Investigation on long-term progressive deformation of engineering slope based on comprehensive monitoring

ZHANG Shi-shu[1] https://orcid.org/0000-0001-5126-8152; e-mail: 1992070@chidi.com.cn

GUO Song-feng[2,3,4*] https://orcid.org/0000-0002-8429-8451; ✉e-mail: guosongfeng@mail.iggcas.ac.cn

QI Sheng-wen[2,3,4] https://orcid.org/0000-0002-0967-7582; e-mail: qishengwen@mail.iggcas.ac.cn

TANG Feng-jiao[2,3,4] https://orcid.org/0000-0001-8944-3155; e-mail: tangfengjiao@mail.iggcas.ac.cn

HU Jin-shan[1] https://orcid.org/0000-0003-1780-3996; e-mail: 2003004@chidi.com

ZHAO Xiao-ping[1] https://orcid.org/0000-0002-4526-8639; e-mail: 2013012@chidi.com

RAN Cong-yan[1] https://orcid.org/0000-0003-2378-5173; e-mail: 2006039@chidi.com

WANG Xin[5] https://orcid.org/0000-0002-6991-9512; e-mail: wangx@mail.neu.edu.cn

ZOU Yu[2,3,4] https://orcid.org/0000-0001-6678-6091; e-mail: zouyu@mail.iggcas.ac.cn

HUANG Xiao-lin[2,3,4] https://orcid.org/0000-0002-6765-3036; e-mail: huangxiaolin@mail.iggcas.ac.cn

ZHENG Bo-wen[2,3,4] https://orcid.org/0000-0002-8204-9654; e-mail: zhengbowen@mail.iggcas.ac.cn

LIANG Ning[2,3,4] https://orcid.org/0000-0002-0320-8451; e-mail: Liangning@mail.iggcas.ac.cn

*Corresponding author

1 Chengdu Engineering Corporation Limited, Power China, Chengdu 610072, China

2 Key Laboratory of Shale Gas and Geoengineering, Institute of Geology and Geophysics, Chinese Academy of Sciences, Beijing 100029, China

3 Innovation Academy for Earth Science, Chinese Academy of Sciences, Beijing 100029, China

4 University of Chinese Academy of Sciences, Beijing 100049, China

5 Key Laboratory of Ministry of Education on Safe Mining of Deep Metal Mines, Northeastern University, Shenyang 110819, China

Abstract: A landslide always results from a progressive process of slope deformation. In recent years, an increasing number of slope instabilities have occurred with regard to human engineering activities such as hydropower or traffic construction in mountainous area, which cause even greater casualties and economic loss compared with the natural hazards. The development of such earth surface process may hold long period with mechanisms still not fully understood. Using monitoring technology is an effective and intuitive approach to assist analyzing the slope deformation process and their driving factors. This study presents

an engineering slope excavated during the construction of Changheba Hydropower Station, which is located in the upper reaches of Dadu River, Sichuan Province, southwest China. The engineering slope experienced and featured a five-year continuous deformation which caused continuous high risks to the engineering activities. We conducted in-depth analysis for such a long-term deformation process based on ground and subsurface monitoring data, collected successive data with a series of monitoring equipment such as automated total station, borehole inclinometers and other auxiliary apparatus, and identified the deformation process based on the comprehensive analysis of monitoring data as well as field investigation. After analyzing the effects of engineering activities and natural factors on the continuous deformation, we found that the overburden strata provided deformable mass while the excavation-produced steep terrain initiated the slope deformation in limit equilibrium state over a long period of time; afterwards, the intense rainwater accelerated slope deformation in the rainy season.

1 Introduction

In general, the rock mass failure is a progressive process of crack initiation, propagation and connection (Bieniawski 1967; Martin 1997; Guo et al. 2015, 2017a, 2020a). Correspondingly, the kinematic release of slope, i.e. landslide, always follows a development procedure involving formation of shear zone or slide surface from initial cracks (i.e., Bjerrum 1967; Einstein 1983; Petley et al. 2004; Guo et al. 2017b, 2017c; Lai et al. 2022).

A number of researchers conducted studies to investigate the intrinsic mechanism of progressive slope failure. Petley et al. (2004) advocated that the first-time landslide failure need a progressive process of shear zone formation. Based on experiments and theoretical analysis, they proposed a conceptual model to depict the progressive failure development of cohesive slope. The conceptual model characterized four stages incorporating microfracture development, shear-surface initiation, growth and formation. They stated that the process of shear surface formation might be intermittent along with changes of external conditions, and the time scale of such process might be as long as hundreds of years. Nevertheless, their model lack verification of detailed monitoring data of slope failure process in field or laboratory. Eberhardt et al. (2014) suggested that deglaciation of the valley below the deformation mass initiate the 1991 Randa rock slide using numerical modelling. Their results also showed that a catastrophic failure was always resulted from progressive degradation and destruction of cohesive elements. Wang et al. (2003) found that the failure characteristics of a heavily jointed rock slope were dominated by the joint quantity and quality. Similar phenomenon was also observed in progressive failure of foliated rock slopes (Adhikary and Dyskin 2007). Some other researchers conducted numerical simulation on the crack growth and ultimate failure process of rock slope (Li et al. 2009; Ma et al. 2013; Scholtes and Donze 2012; Zhang et al. 2013, 2015).

A variety of techniques have been put forward to track the slope deformation process (Gili et al. 2000; Wu et al. 2019). Luo and Zhang (2016) conducted a series of centrifuge model tests combined with image capture and displacement measurement system to study the slope failure mechanism subjected to drawdown of water level. They found that the slip surface was developed from the top downwards due to drawdown. Darban et al. (2019) analyzed the failure mechanism of unsaturated granular slopes subjected to continuous rainfall using small-scale experiments monitored by miniaturized sensors and optical fibers. They found the slope collapsed only when the deepest soil layer was in full saturation, and characterized such phenomenon by undrained instability mechanism. Meanwhile, some non-contact techniques have been adopted to obtain the deformation information of actual slope in field. Yin et al. (2010) analyzed the ground deformation of a natural landslide in southwest China using GPS and InSAR data, on the basis of which they discussed its driving factors. Stock et al. (2012) adopted high-resolution photography, video, and laser scanning to analyze the progressive failure of a sheeted rock slope in USA. Similar techniques were also put into use in some other slope failure cases (Royan et al. 2015; Riva et al. 2018). These noncontact monitoring techniques are mostly accessible and largely promote the researches of geological disaster, however, have also some limitations, e.g. only presenting surface deformation and difficult to obtain real-time deformation.

As human activities increase obviously in the past decades, numerous engineering slopes have been formed and most of them experience complicated disturbances and are metastable and deformable (Qi et al. 2015; Wang et al. 2020; Guo et al. 2020b). Fortunately, these risks are always conspicuous and people can employ monitoring and early warning measures with more comprehensive measurement techniques. A few cases are reported in different types of engineering practices, such as open-pit mine, dam, and slope induced by water fluctuation of the reservoir (He et al. 2004; Wu et al. 2005; Qi et al. 2006; Wang et al. 2010; Chen et al. 2018; Clarkson et al., 2021). Nevertheless, the deformation mechanism of engineering slopes resulting from human activities are always complicated and still not fully understood, which frequently causes huge life and economic loss (Temme et al. 2020).

In this study, the progressive deformation process of an excavated slope was dissected in detail based on comprehensive monitoring of both surface and underground deformation for over 5 years. The monitoring data is analyzed in detail, and the deformation mechanism is discussed linked to engineering and natural driving factors.

2   Background of the Engineering Slope

2.1 Brief introduction of the project

Changheba Hydropower Station is located in Kangding County, Sichuan Province, Southwest China. With a capacity of 2600 MW, this hydropower station is one of the large-scale hydroelectric power stations in the Dadu River Basin. The reservoir's normal water level and total storage capacity are 1,690 m and 1,075,000,000 m³ respectively.

Rock-fill dam with gravel soil core is adopted, the height of which is 240 m. Consequently, a huge amount of standard-compliant gravel soils, roughly 4,300,000 m³, should be prepared to construct the dam as the core wall material. The Tangba earth quarry, a natural slope with available impervious materials of about 4,400,000 m³ and close to the dam site, is selected for material supply. The gravel soils excavation sustained for nearly three years from Sept. 2013 to May. 2016. An engineering slope was thus formed with height of nearly 500 m and slope ratio larger than 1:1. The elevation of slope is between 2,525 m and 2,008 m (see Fig. 1). A large number of fresh fractures were observed during and after the excavation activities, and the stability of such a high engineering slope was an urgent issue to be solved.

2.2 Engineering geological conditions

The topography of natural Tangba earth quarry is generally characterized as funnel-shaped, with an overall slope angle of 20° ~ 30°. According to the topographic features, the quarry field can be divided into three sub zones, separated by ridges (Fig.1). For the three slopes, Slope II is the most dangerous one with an overall slope angle of 28°~35° and a height of

Fig. 1 Slope zoning of the Tangba earth quarry of Changheba Hydropower Station.

over 500 m. After excavation, the overall slope angle reached up to 45° ~ 65°, and a groove-like topography was formed, which was prone to be a catchment channel.

The bedrocks are thin to medium-bedded limestone and slate of Devonian (D12) with a strike direction of 10°~50° and nearly vertical stratigraphical dip angle. The rock masses are completely highly weathered under the shallow layer with a thickness of 15~25 m. The Quaternary deposits incorporated mainly fluvioglacial deposition and partially moraine soil as well as diluvial-residual detritus soil, with relatively fine particles and loose to slightly dense structure. The thickness of Quaternary deposits varied from 15 ~ 40 m. A series of laboratory tests were conducted to obtain the physical and mechanical properties of the fluvioglacial deposit and moraine soil (Table 1).

Table 1 Physical and mechanical properties of the fluvioglacial deposit and moraine soil of the Tangba earth quarry slope

The physical and mechanical properties			Value
Dry density (g/m³)			1.88 ~ 1.98
Natural moisture content (%)			3.2 ~ 9.4
The average void ratio			0.408
The plasticity index			12~15
Deformation intensity parameters	Natural consolidated-quickly shear test	c (kpa)	35 ~ 50 (43.3)
		φ (°)	25.6~28.4 (26.9)
	Saturated consolidated-quickly shear test	c (kpa)	10~60 (38.3)
		φ (°)	24.2~27.5 (25.5)

Note: The values in in brackets mean average.

The study area had a dual hydrogeological structure, composed of pore phreatic water and perched water in the upper quaternary overburden layer, and fissure water in the bedrock layer. According to the investigations during exploration and excavation, there is no stable groundwater in the quaternary layer with only moist soil existing locally. Some water seepage appeared during reinforcement.

2.3 Deformation process of engineering slope during and after excavation

As depicted in Fig. 1, the Tangba earth quarry could be divided into three slopes of I, II, and III from downstream to the upper stream. The slopes I and III were basically stable for the relatively gentle terrain, while the deformation mainly occurred in slope II.

Quarry excavation activities started at the elevation of 2,260 m in Sept. 2013. The maximum gradient of excavated slope was nearly 1:0.5, and no support measures were conducted at the beginning period. The initial fractures were observed initially on Feb. 24th, 2014 at an elevation between 2,235 ~ 2,267 m. The tension fissures opened up to 50 cm in the posterior border. The deformation area extended rapidly to elevations of 2,118 m and 2,381 m at the bottom and top boundary, respectively, and multi persistent slide surfaces were formed gradually with shear outlets at the elevation between 2,118 m and 2,210 m (Fig. 2) at the end of Mar. 2014.

In Apr. 2014, the deformation mass at the elevation between 2,210 m and 2,385 m started to slide with a rate of 20~30 mm per day. The deformation rate increased up to 120 mm per day during the rainy season. The boundary of deformation mass reached to elevation of 2,405 m in Oct. 2014. The dam fillings and quarry excavation activities finished on May 9th, 2016. After that, the upper part of slope (higher than elevation of 2,360 m) was reinforced in Sept. 2016 and could basically keep the

Fig. 2 Deformation conditions of the Tangba earth quarry slope in Mar. 2014. (a) Shear outlets at the elevation of 2,120.0 m; (b) Shear outlets at the elevation of 2,210.0 m.

slope stable, while the stability of the lower part slope was in a critical state, with a deformation rate of 1.3 mm per day according to the monitoring data from 2016 to 2017.

According to the planning, the quarry area would be developed for resettlement and cultivation, and thus treatments should be put forward to ensure the slope stability. Slope flattening started at the lower part (lower than elevation of 2,360 m) in Mar. 2018, and yet no strong enough supports were conducted simultaneously. As a consequence, the deformation of the slope increased rapidly, and a landslide occurred eventually at the elevations of 2,320m ~ 2,360m in July 2018. The progressive failure will be depicted quantitatively based on a comprehensive monitoring system in the next section.

3　Main Monitoring Measures

3.1 Monitoring apparatus

Different approaches were employed to obtain the real-time deformation data automatically. An automated total station system was adopted to monitor the slope surface deformation, while a number of borehole inclinometers were used to obtain the subsurface deformation. Besides, some auxiliary

apparatus were also employed to monitor stress and pore water pressure in the slope involving of soil pressure cells, reinforcement stress gauges, and osmometers.

3.2 Layout of monitoring apparatus

The automated total station system incorporated a series of fixed prism observation stations. A total of seventy-three devices were installed between 2016 and 2018, among which about thirty-five devices' data were available. Fig.3a shows the layout of observation points in the elevation between 2,230 m and 2,450 m, which indicates that three slope parts were monitored from slope top to toe. At the slope top area with elevation of about 2,450 m, several devices were set up to identify the top boundary of the deformation body (Zone A). Three sections of devices were set up to obtain the deformation condition of the slope with elevation between 2,350 m and 2,435 m (Zone B). Moreover, additional scattered devices were set up in the lower part of the slope with elevation between 2,230 m and 2,350 m (Zone C). Besides, one more observation point was arranged in the rear slope with elevation of about 2,525 m.

To monitor the interior deformation of slope, over twenty sets of inclinometer tubes were put to use in the slope area. The available interior monitoring
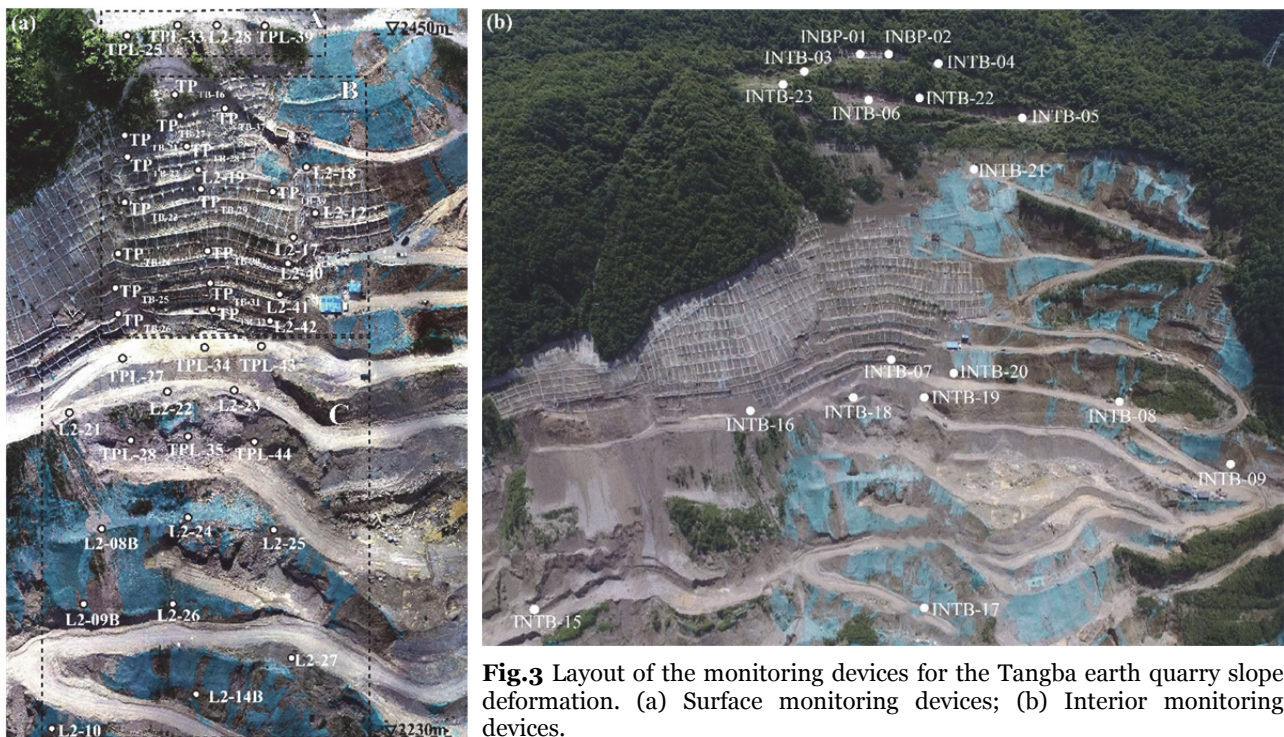

Fig.3 Layout of the monitoring devices for the Tangba earth quarry slope deformation. (a) Surface monitoring devices; (b) Interior monitoring devices.

devices basically covered the whole slope (Fig. 3b).

4 Progressive Deformation Features based on Monitor Results

4.1 Deformation behavior on slope surface

The displacement data were recorded and collected for both the surface and subsurface of slope using the installed monitoring apparatus. As mentioned, a few devices were invalid due to lack of maintenance from 2016 to 2018, and thus some new devices were installed in 2018. Therefore, more data were available after 2018 compared with that during period of 2016-2018. The monitoring data of slope surfaces at varied elevations are shown in Fig. 4. The ΔX and ΔY denote the displacement inclined and trend to slope, respectively, while ΔH denotes deformation at vertical direction. The positive values of ΔX, ΔY, ΔH indicate the displacement toward slope aspect, upstream and downward, respectively. It can be seen that the displacements occurred mainly in the ΔX and ΔH directions. The displacements of monitoring point larger than 1 m are marked as red and green solid circles. The red and green represent the displacement in the period of Jun. 2016 - Oct.

2018 and Nov. 2018 - Sep. 2019, respectively. The larger the radius of the circle, the larger the displacement at the location. The monitoring data according to six devices in the period of Jun. 2016 - Oct. 2018 indicates that the maximum displacement of over 10 meters occurred in the top of zone B at an elevation around 2,410 m (see the biggest red solid circles in Fig. 4). During the period of Nov. 2018 to Sep. 2019, the maximum displacement of over 7.0 m also occurred in the top of zone B (Device No. TP$_{TB-37}$) as well as the slope crest zone A at the elevation around 2,440 m (Device No. TPL-33), and some large deformation with the displacements over 1.0 m occurred in the lower part of the slope at the elevation of 2,265~2,291 m (devices Nos. L2-22, TPL-28, L2-08B, L2-24, L2-25, L2-09B, L2-26). It indicates clearly that the deformation area expanded after the slope flattening activities in 2018, i.e., the upper boundary of deformation expanded from elevation of 2410 m to 2440 m, and the lower part (Zone C) began to accelerate continuous deformation.

4.2 Deformation in the subsurface of slope

The deformation status inside the slope are reflected by the monitoring data of inclinometer tubes.
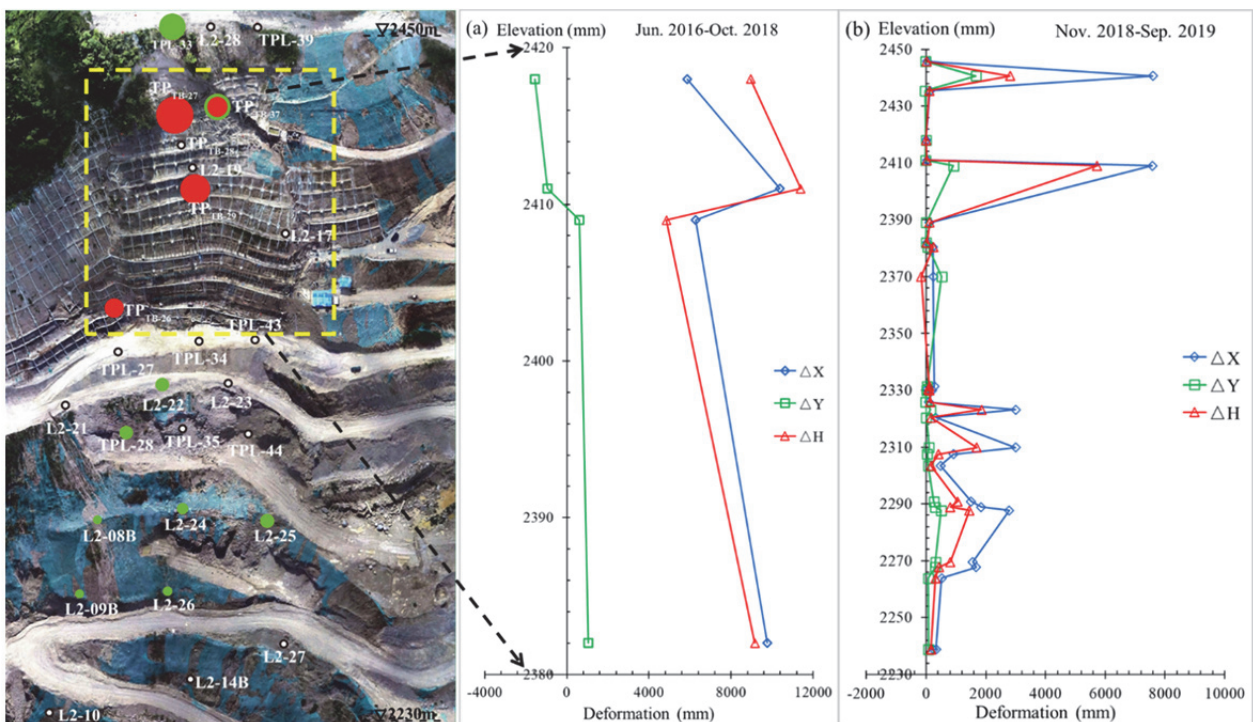

Fig. 4 Continuous monitoring results of Tangba earth quarry slope surface deformation during (a) period from Jun. 2016 to Oct. 2018 and (b) period from Nov. 2018 to Sep. 2019. (Displacements of monitoring point larger than 1 m are denoted as red and green solids respectively, and the larger the radius, the larger the displacement.)

The positive values of data indicate the displacement toward free face. The monitoring results show that the displacements in the slope crest (zone A) are less than 3.0 cm at depth of 0-20 m during the period of 2015 to 2019. The monitoring data at the toe of zone B (INTB-20 with the borehole head at the elevation of 2234.33 m) show that the maximum displacement of 1.3 cm occurred at the borehole depth of 1.0 m in the period of Dec. 2018 to Sep. 2019 (the whole monitor depth is about 42.0 m).

Compared with those in Zone A, the monitoring data indicated that a larger interior deformation occurred in zone B (i.e., INTB-17 and INTB-18). Device No. INTB-17 (at the elevation of 2,235.35 m) has a maximum displacement of 146.50 mm toward the free surface at the borehole depth of 15m-20m in the period from Jan. 2019 to Oct. 2019 (Fig. 5a). It indicates that the sliding plane of this location are formed at depth of 20 m during this period. The maximum displacement of device No. INTB-18 (the borehole head at the elevation of 2,320 m) is about 100.90 mm toward the free surface at the borehole depth of 13.5 m from Dec. 2018 to Mar. 2019 (Fig. 5b).

Thus the depth of the slide plane in this borehole was about 13.5m.

4.3 Comprehensive analysis of the deformation process

The upper section of the slope zone B (higher than El 2360) was supported at the end of excavation in May 2016, and after that, the supported zone B was basically stable during the period of May 2016 to Mar, 2018. On the other hand, a slow creep deformation occurred in the zone at elevation of 2,100~2,360 m, which indicated that it was in a critical equilibrium state in the same period.

For the safety of cultivated land utilization, the deformed blocky rock masses and loose debris should be removed on the shallow surface of slope. The slope flattening and reinforcement for the lower section of zone B (lower than El 2360m) began in Mar. 2018. The excavation activities at elevation of 2,330~2,360 finished on May 12th 2018, and then some temporary supports were installed on shallow superficial layer of slope. From Jul. 8th to 17th 2018, the excavation
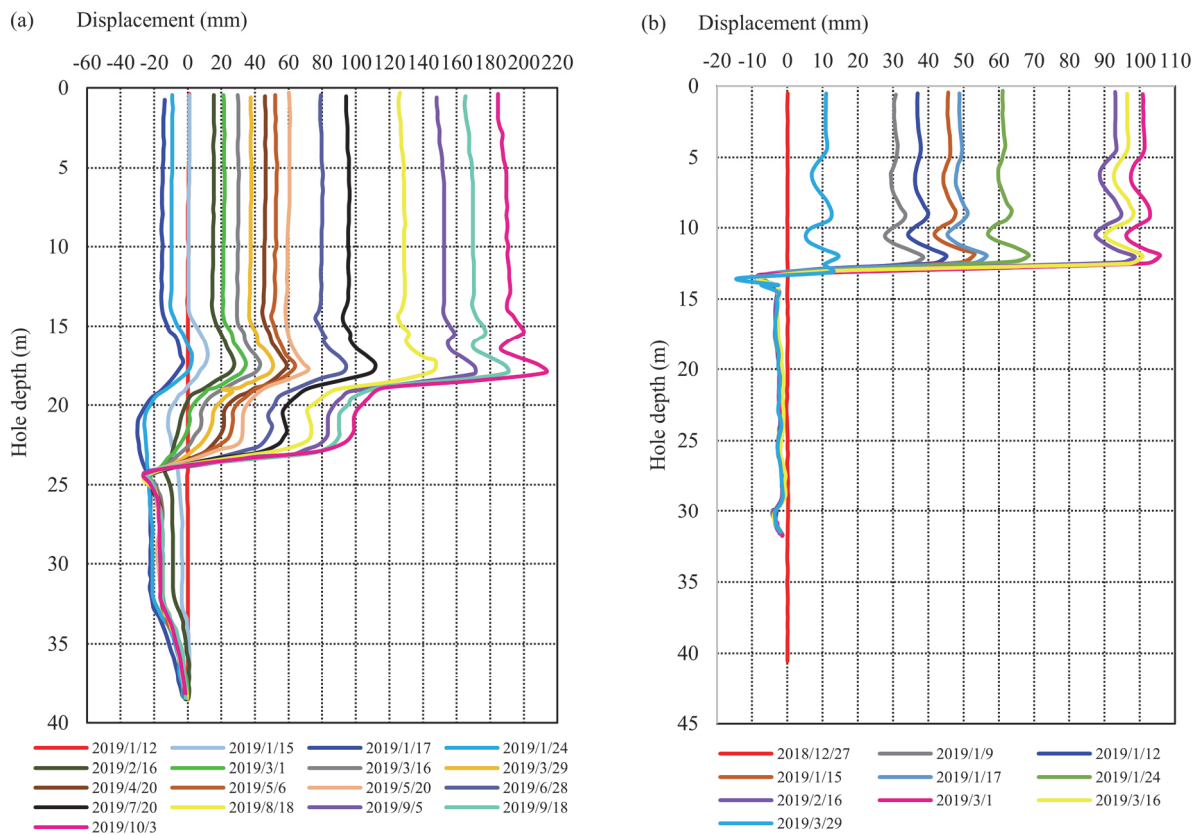

Fig. 5 Displacement at varied depth in subsurface of slope in 2019. (a) the lower location of zone B; (b) the upper location of zone B.

activities continued at the elevation of 2,330 m~2,320 m. Obvious fractures as well as increasing monitoring displacements appeared immediately and expanded progressively. The process of progressive failure is shown in Table 2 and Fig. 6a.

Following the slope failure process depicted in Table 2, a successive deformation occurred in the left upper part at elevation of 2,440~2,490m after 5-days persistent precipitation from Sept. 29th to Oct. 4th 2018 (Fig.6b). The deformation rate were about 50~100 mm/d in Oct. 1st ~ 3rd, and reached 200-460 mm/d in Oct. 4th ~7, 30~160 mm/day in Oct. 8th ~25th, 5~22 mm/d after Oct. 26th 2018. It indicated that the new deformation event also experienced a process of fracture initiation and propagation, slip initiation and acceleration, post-peak slippage, and residual deformation. As of Dec. 18th, 2018, the monitoring data showed that the slope had a downward displacement of 3.1 m at elevation of 2481m, and 6.32 m at elevation of 2,409 m. Besides, some initial fractures occurred at elevation 2,490~2,520 m, while no deformation signs were observed beyond elevation 2,520 m.

The slope experienced a secondary sliding event at elevation between 2,440 and 2,475 m during the period from Nov. 2018 to Oct. 2019. Most of the support facilities in this area entirely failed and the deformation reached up to 10.92m and 4.46m at x and z-direction, respectively. Another obvious slipping event occurred in at elevation between 2,260 and 2,440 m. This sub zone featured fluctuant deformation, i.e. creeped most of time while had a sharp slippage events abruptly. The total displacement of this zone was 10.72 m and 8.08 m at x and z-direction respectively. The monitoring data showed that the slope was in a creep state in the range of El 2,260~2,200 m.

The observed phenomenon as well as monitoring data show the slope deformation is a progressive process, which incorporates fracturing initiation and propagation, slippage initiation and acceleration, peak and residual deformation. In addition, the deformed mass features multi-slipping upward in adjacent regions, which can be classified as a typical retrogressive landslide. The deformation process also features with a rapid deformation that always accompanied at creep stage.

5   Discussion on the Mechanism of Slope Deformation

To understand the deformation mechanism of slope, the possible influencing factors that may accelerate the failure process were analyzed. First of all, the engineering geological condition was considered as a basic factor. Moreover, the triggering factors involving of engineering disturbance and

Table 2 Process of progressive failure of Zone II of the Tangba earth quarry in 2018

Deformation stage	Time range	Deformation phenomenon	Deformation rate (mm/d)	
Initial creep stage	Before 2018/7/19	a number of fresh fissures were observed on the slope at an elevation of 2,340~2,410 m	8 (maximum)	
Sliding surface formation	2018/7/19 -8/6	A total of 28 fresh fissures were observed according to the site survey on Aug. 5th. Some fissures have openness of 5~20cm, which confined the boundary of deformation mass. The support structures in the deformation mass were damaged and even failed. It indicated that a connected slide surface is formed gradually. During this period, the slope deformed or slipped with a stable rate.	2018/7/23	35 (maximum)
			2018/8/4	73 (maximum)
Unstable slip stage	2018/8/6 -8/13	The deformation rate started to accelerate rapidly on Aug. 6th	2018/8/6	400-500
		The peak of the deformation rate occurred on Aug. 8th 2018	2018/8/8	1800 (maximum)
		The slope is in a violent sliding phase	2018/8/7-8/13	400~1200
Post-peak slip	2018/8/13 -8/28	The frame girder, and anchor cable along the boundary of deformation mass had been broken completely, especially the leading edge where the anchor cable had a dislocation of 2.5 m	2018/8/13-8/28	100~200
Residual stage	2018/8/28 -9/15	The total deformations were 8.9 m and 5.6 m along the h and x-direction of the back edge, and 3.0 m and 11.0 m respectively at the front edge. The dip angle of slope cliff was about 60° as surveyed on Sept. 3rd 2018	40~90	

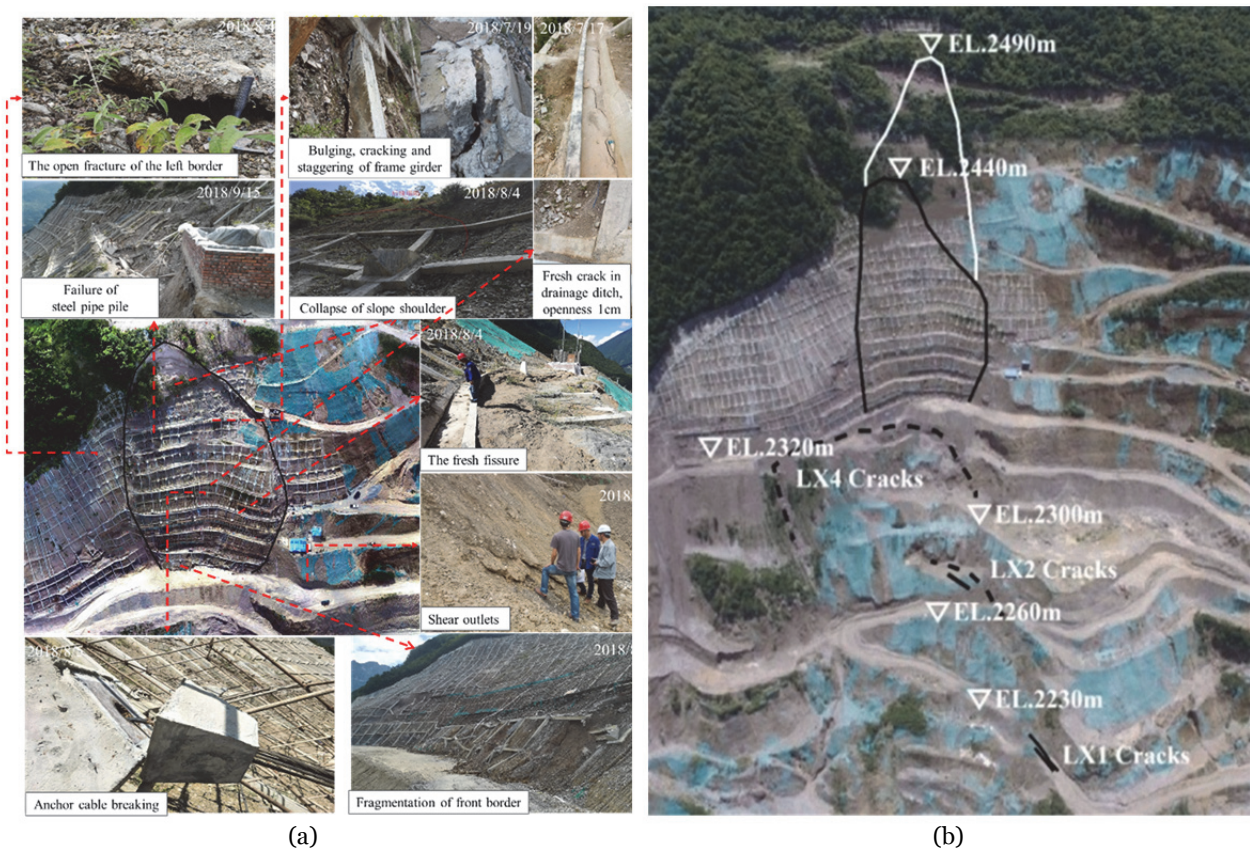**Note:** *All deformation directions are the x-direction.

Fig. 6 Deformation features based on field investigation of the Tangba earth quarry slope from July to October in 2018. (a) The fracturing process. (b) The eventual failure area.

rainfall are taken into accounts.

5.1 Terrain and lithology factors

The terrain condition is an essential prerequisite for the slide-prone trend of a slope. The Tangba soil yard was a steep slope, especially after excavation. The highest gradient of excavated slope reached up to 1:0.5, and the slope height reached 500 m. It was an enormous challenge to keep such an overburden slope under stable status for long time.

The lithological association was another basic factor for the slope deformation. The deposits incorporated mainly ice-water accumulation detritus soil with high clay content. Thus, the overburdened materials were characterized by water sensitivity and creep behaviors. The crack and pore structures that developed in overburden deposits acted as a permeability pathway for rainwater from the surface to a soil-rock interface.

5.2 Engineering activities

The natural deposit slope was initially excavated for dam fillings, which lasted nearly 3 years from July 2013 to May 2016. Damages initiated closely following the excavation activities in Feb. 2014, and extended rapidly beyond the designed scope of excavation site one month later. The spreading deformation along with the excavation threatened the safety of engineering activities as well as the residents. Thus, some temporary treatments were put forward during excavation. The slope deformation slowed down after the excavation finished but had been creeping without systematic support measures.

For resettlement and cultivation in this area as planned, the treatments were conducted again to ensure the slope stability. In Mar. 2018, the height of slope flattening reached up to 40 m (elevation between 2,360m and 2,320m), but no supports were installed in this period. The monitoring data of instruments showed obvious deformation and fresh fractures were detected new fractures around the slope. After that, the slope experienced long-term continuous deformation.

A conclusion can be drawn that the excavation

activities initiated the slope deformation. The support treatments, on the other hand, played a role in retarding the deformation process.

5.3 Precipitation

This slope deformation process characterized with a fluctuating deformation rate. The rate did not increase or decrease monotonously, however, the relatively rapid deformation alternated with slow deformation. We deliberated the mechanism that promoted such occurrence based on monitoring data.

According to the monitoring data, the top of zone B had a significant displacement (Fig. 5). Thus, we analyzed the deformation process of the monitoring point in this area (Device No. TP$_{TB-37}$ at elevation of 2,410m) from Apr. to Sep. 2018 (Fig.7). It indicates that in this period, the deformation of slope had three obvious rapid rising stages. The first time occurred in the period from Jun. 6th to 27th, 2019 with displacement of about 525.94 mm, the second time occurred in the period from Jul. 5th to 15th 2019 with displacement of about 1228.77 mm, and the third time occurred in the period from Aug. 1st to 18th 2019 with displacement of about 1319.23 mm.

The comparison between precipitations and slope deformation process at the same period are shown in Fig. 7. It shows that the rainy season began in April, but the first continuous rainstorm occurred in June with top precipitation as high as 35 mm in twenty-four hours. The comparison shows that the monitoring deformation derived from Device No. TP$_{TB-37}$ had a first rapid rise closely following the heavy or prolonged rain in Jun. 2019. After June, the monitoring deformation experienced a stepped

growth consistent with the period of high precipitation. Moreover, we analyzed another monitoring deformation data of Device No. L2-22 at elevation of 2,323m (Fig. 7). It reveals that the moment that deformation initiated was basically in accordance with that recorded by Device No. TP$_{TB-37}$ as well as the maximum precipitation. Afterwards, a continuous deformation occurred during the rainy season.

Based on the deformation at different depth of a borehole derived from Device No. INTB-17 (the location can be tracked in Fig. 5a), the comparison between the interior displacement at different depths and rainfall in 2019 are shown in Fig. 8. The results show that the displacements slightly increased with a rate of about 8 mm per month before June, while with much higher rates of about 40 mm per month during Jun. to Sept. for the points with depth shallower than 20m. On the other hand, the monitoring data had barely changed at depth of 25m, which indicated the depth of sliding face was between 20m ~ 25m in this borehole. As the precipitation increased obviously in the period between Jun. and Sept. 2019, the deformation interior slope also increased.

The comparison of monitoring data signified that the slope deformation and had a positive correlation with the precipitation process. Meanwhile, no engineering activities or other events that affected stability were put forward in 2019. Thus, rainwater was regarded as the facultative factor that promoted the deformation initiation and growth in this period. The rainwater permeated the rock-soil interface through cracks, which can reduce the effective stress and weaken the material strength of the interface layer. This process gradually weakened slope
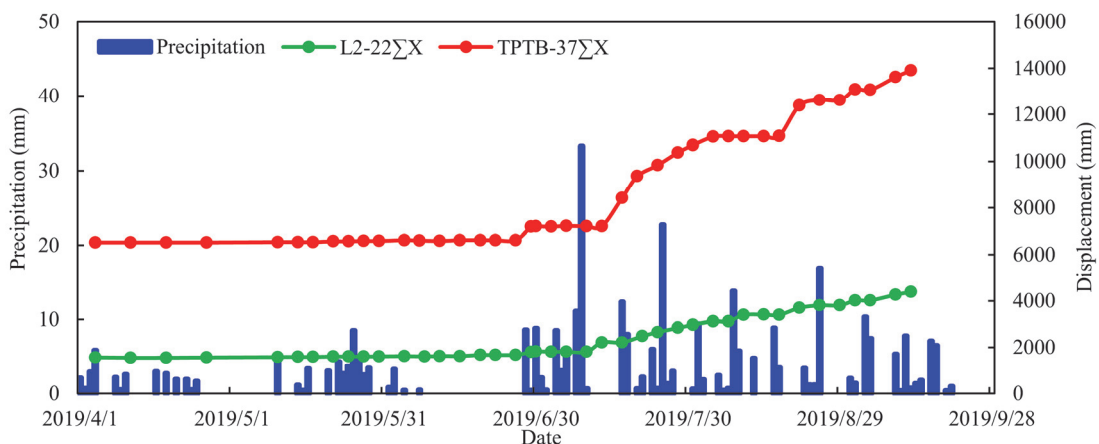

Fig. 7 Comparison between precipitations and cumulative deformation at direction of slope free surface (∑X) of TPTB-37 in zone B and L2-22 in zone C between April to September in 2019.
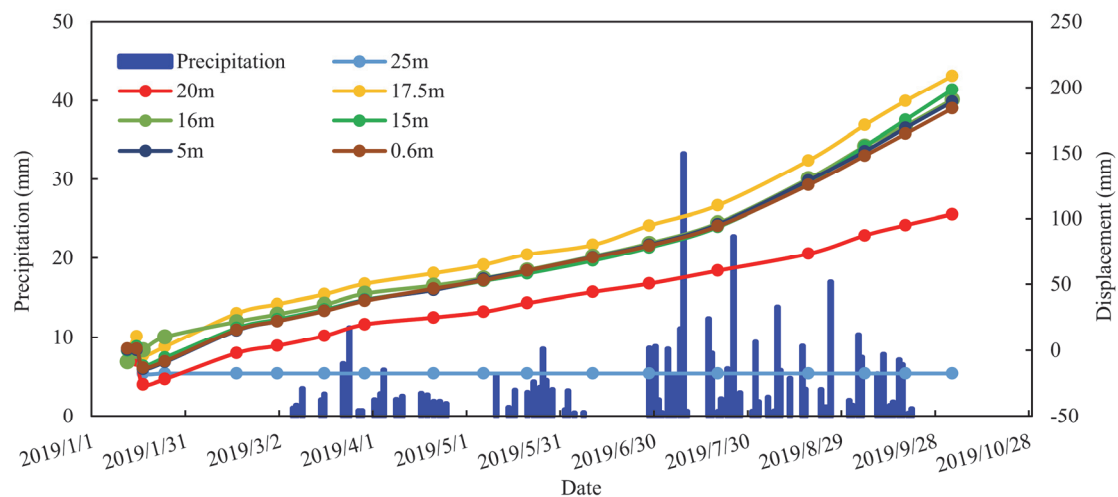
Fig. 8 Comparison between the interior displacement at different depths as well as precipitation of INTB-17 in zone C during January to October in 2019.

instability, and thus the deformation had a stepped or continuous increase following the rainfall.

Through the above analysis, we can well understand that the excavation activities and rainwater led to the long-term progressive deformation of a slope. Firstly, the engineering excavation prompted the slope failure in the early stage of the dam filling period before 2016, and afterwards slope stayed in the limit equilibrium state until the engineering actives at the beginning of 2018. The slope treatment, starting with excavation, extended deformation and caused typical retrogressive landslides in 2018. Latterly, the rainwater became the primary factor in promoting slope deformation, which can be confirmed by the close correlation of deformation data and precipitation in 2019. This case showed that the slope deformation might be intermittent along with changes of external conditions, which provides a practical verification of Petley's model (Petley et al. 2004).

6 Conclusion

The slope instability is a progressive failure process subjected to natural or engineering disturbance. The appropriate measurements can provide quantitative information for researchers to better understand such processes, conduct the stability analysis of slope, and early warning of landslide. This paper presents a comprehensive measurement method to reach both surface and subsurface deformation of a slope. The procedure was applied to a quarry excavation slope, and the deformation data were collected over a period of five years. Thus, the mechanism of such a long-term development of slope deformation can be analyzed in detail.

The steep terrain and overburden strata provide the basic slide-prone condition. Initially, the quarry excavation was the major factor that caused slope instability in the early stage of 2016, and the slope stayed in the limit equilibrium state as the excavation finished for nearly two years. The slope deformation accelerated again when the slope flattening activities were carried out in 2018. Afterwards, the rainwater turned into the primary driving factor for the intermittent acceleration of slope deformation. This research introduces a typical slope deformation model influenced by both natural and engineering aspects, which can provide experiences for comparable projects. It indicates that the engineering activities should be conducted with scientific design, and appropriate support measures should be put forward as soon as possible to avoid creep deformation.

Acknowledgements

References

Adhikary DP, Dyskin AV (2007) Modelling of progressive and instantaneous failures of foliated rock slopes. Rock Mech Rock Eng 40(4): 349- 362.
https://doi.org/10.1007/s00603-006-0085-8

Bieniawski ZT (1967) Mechanism of brittle fracture of rock: part I—theory of the fracture process. Int J Rock Mech Min Sci Geomech Abstr 4: 395-406.
https://doi.org/10.1016/0148-9062(67)90030-7

Bjerrum L (1967) Progressive failure in slopes of overconsolidated plastic clay and clay shales. J Soil Mech Found Div Am Soc Civ Eng 93: 1-49.
https://doi.org/10.1061/JSFEAQ.0001017

Clarkson L, Williams D, Seppälä J (2021). Real-time monitoring of tailings dams. Georisk 15(2): 113-127.
https://doi.org/10.1080/17499518.2020.1740280

Chen M, Lv P, Zhang S, Chen X, et al. (2018) Time evolution and spatial accumulation of progressive failure for Xinhua slope in the Dagangshan reservoir, Southwest China. Landslides 15: 565-580.
https://doi.org/10.1007/s10346-018-0946-8

Darban R, Damiano E, Minardo A, et al. (2019) An experimental investigation on the progressive failure of unsaturated granular slopes. Geosci 9: 63.
https://doi.org/10.3390/geosciences9020063

Eberhardt E, Stead D, Coggan JS (2004). Numerical analysis of initiation and progressive failure in natural rock slopes- the 1991 Randa rockslide. Int J Rock Mech Min 41: 69-87.
https://doi.org/10.1016/S1365-1609(03)00076-5

Einstein HH, Veneziano D, Baecher GB, et al. (1983). The effect of discontinuity persistence on rock slope stability. Int J Rock Mech Min 20(5): 227-236.
https://doi.org/10.1016/0148-9062(83)90003-7

Gili JA, Corominas J, Rius J (2000) Using global positioning system techniques in landslide monitoring. Eng Geol 55(3): 167-192.
https://doi.org/10.1016/S0013-7952(99)00127-1

Guo S, Qi S (2015) Numerical study on progressive failure of hard rock samples with an unfilled undulate joint. Eng Geol 193: 173-182.
https://doi.org/10.1016/j.enggeo.2015.04.023

Guo S, Qi S, Zhan Z, et al. (2020a) Numerical study on the progressive failure of heterogeneous geomaterials under varied confining stresses. Eng Geol 269: 105556.
https://doi.org/10.1016/j.enggeo.2020.105556

Guo S, Qi S, Saroglou C (2020b) A-BQ, a classification system for anisotropic rock mass based on China National Standard. J Cent South Univ 27: 3090-3102.
https://doi.org/10.1007/s11771-020-4531-7

Guo S, Qi S, Zhan Z, et al. (2017a) Plastic-strain-dependent strength model to simulate the cracking process of brittle rocks with an existing non- persistent joint. Eng Geol 231: 114-125. https://doi.org/10.1016/j.enggeo.2017.10.008

Guo S, Qi S, Yang G, et al. (2017b) An analytical solution for block toppling failure of rock slopes during an Earthquake. Appl Sci 7: 1008.
https://doi.org/10.3390/app7101008

Guo S, Qi S, Zou Y, et al. (2017c) Numerical studies on the failure process of heterogeneous brittle rocks or rock-like materials under uniaxial compression. Materials 10: 378.
https://doi.org/10.3390/ma10040378

He X, Yang G, Ding X, et al. (2004) Application and evaluation of a GPS multi- antenna system for dam deformation monitoring. Earth Planets Space 56: 1035-1039.
https://doi.org/10.1186/BF03352545

Lai Q, Zhao J, Huang R, et al. (2022) Formation mechanism and evolution process of the Chada rock avalanche in Southeast Tibet, China. Landslides 19:331-349.
https://doi.org/10.1007/s10346-021-01793-4

Li L, Tang C, Zhu W, et al. (2009) Numerical analysis of slope stability based on the gravity increase method. Comput Geotech 36: 1246–1258.
https://doi.org/10.1016/j.compgeo.2009.06.004

Luo F, Zhang G (2016) Progressive failure behavior of cohesive soil slopes under water drawdown conditions. Environ Earth Sci 75: 973. https://doi.org/10.1007/s12665-016-5802-3

Ma K, Tang C, Li C, et al. (2013). 3D modeling of stratified and irregularly jointed rock slope and its progressive failure. Arab J Geosci 6: 2147-2163.
https://doi.org/10.1007/s12517-012-0578-6

Martin C (1997). Seventeenth Canadian geotechnical colloquium: the effect of cohesion loss and stress path on brittle rock strength. Can Geotech J 34 (5): 698-725.
https://doi.org/10.1139/t97-030

Petley D, Higuchi T, Petley D, et al. (2004). Development of progressive landslide failure in cohesive materials. Geology 33(3): 201-204. https://doi.org/10.1130/G21147.1

Qi S, Li X, Guo S, et al. (2015) Landslide- risk zonation along mouontainous highway considering rock mass classification. Environ Earth Sci 74: 4493-4505.
https://doi.org/10.1007/s12665-015-4453-0

Qi S, Yan F, Wang S, et al. (2006) Characteristics, mechanism and development tendency of deformation of Maoping landslide after commission of Geheyan reservoir on the Qingjiang River, Hubei Province, China. Eng Geol 86: 37-51.
https://doi.org/10.1016/j.enggeo.2006.04.004

Riva F, Agliardi F, Amitrano D, et al. (2018) Damage-based time-dependent modeling of paraglacial to postglacial progressive failure of large rock slopes. J Geophys Res-Earth 123: 124-141.
https://doi.org/10.1002/2017JF004423

Royan MJ, Abellan A, Vilaplana JM (2015) Progressive failure leading to the Dec. 3rd 2013 rockfall at Puigcercos scarp (Catalonia, Spain). Landslides 12: 585-595.
https://doi.org/10.1007/s10346-015-0573-6

Scholtes L, Donze F (2012) Modelling progressive failure in fractured rock masses using a 3D discrete element method. Int J Rock Mech Min 52: 18-30.
https://doi.org/10.1016/j.ijrmms.2012.02.009

Stock GM, Martel S, Collins BD, et al. (2012) Progressive failure of sheeted rock slopes: the 2009-2010 Rhombus Wall rock falls in Yosemite Valley, California, USA. Earth Surf Proc Land 37: 546-561.
https://doi.org/10.1002/esp.3192

Temme A, Guzzetti F, Samia J, et al. (2020) The future of landslides' past- a framework for assessing consecutive landsliding systems. Landslides 17:1519-1528.
https://doi.org/10.1007/s10346-020-01405-7

Wang C, Tannant DD, Bicanic N (2003). Numerical analysis of the stability of heavily jointed rock slopes using PFC2D. Int J Rock Mech Min 40: 227-236.
https://doi.org/10.1016/S1365-1609(03)00004-2

Wang J, Gao J, Liu C, et al. (2010). High precision slope deformation monitoring model based on GPS/Pseudolites technology in open-pit mine. Min Sci Tech 20: 126-132.
https://doi.org/10.1016/S1674-5264(09)60173-3

Wang Z, Gu S, Zhang W (2020) Influence of excavation schemes on slope stability: A DEM study. J Mt Sci 17(6): 1509-1522.
https://doi.org/10.1007/s11629-019-5605-6

Wu F, Qi S, Lan H (2005) Mechanism of uplift deformation of the dam foundation of Jiangya Water Power Station, Hunan Province, P.R. China. Hydrogeol J 13: 451-466.
https://doi.org/10.1007/s10040-004-0374-9

Wu H, Guo Y, Xiong L, et al. (2019) Optical fiber-based sensing, measuring, and implementation methods for slope deformation monitoring: A review. Ieee Sens J 19(8): 2786-2800. https://doi.org/10.1109/JSEN.2019.2891734

Yin Y, Zheng W, Liu Y, et al. (2010) Integration of GPS with InSAR to monitoring of the Jiaju landslide in Sichuan, China. Landslides 7(3): 359-365.
https://doi.org/10.1007/s12583-010-0137-6

Zhang K, Cao P, Bao R (2013) Progressive failure analysis of slope with strain-softening behavior based on strength reduction method. J Zhejiang Univ-Sci A 14(2): 101- 109.
https://doi.org/10.1631/jzus.A1200121

Zhang K, Cao P, Meng J, et al. (2015) Modeling the progressive failure of jointed rock slope using fracture mechanics and the strength reduction method. Rock Mech Rock Eng 48: 771-785.
https://doi.org/10.1007/s00603-014-0605-x